Open access • Journal Article • DOI:10.1063/1.2338602

Growth of p-type and n-type m-plane GaN by molecular beam epitaxy — Source link

Melvin McLaurin, Tom Mates, Feng Wu, James S. Speck

Published on: 22 Sep 2006 - Journal of Applied Physics (American Institute of Physics)

Topics: Full width at half maximum and Molecular beam epitaxy

Title

Growth of p-type and n-type m-plane GaN by molecular beam epitaxy

Journal

Journal of Applied Physics, 100(6)

ISSN

0021-8979

Authors

McLaurin, M
Mates, T E
Wu, F
et al.

Publication Date

2006-09-01

Peer reviewed

Growth of *p*-type and *n*-type *m*-plane GaN by molecular beam epitaxy

M. McLaurin,[a] T. E. Mates, F. Wu, and J. S. Speck
Materials Department, University of California, Santa Barbara, California 93106
and ERATO/JST UCSB Group, University of California, Santa Barbara, California 93106

(Received 8 March 2006; accepted 26 May 2006; published online 22 September 2006)

Plasma-assisted molecular beam epitaxial growth of Mg-doped, *p*-type and Si-doped, *n*-type *m*-plane GaN on 6*H* *m*-plane SiC is demonstrated. Phase-pure, *m*-plane GaN films exhibiting a large anisotropy in film mosaic ($\sim 0.2°$ full width at half maximum, x-ray rocking curve scan taken parallel to $[11\bar{2}0]$ versus $\sim 2°$ parallel to [0001]) were grown on *m*-plane SiC substrates. Maximum hole concentrations of $\sim 7\times 10^{18}$ cm^{-3} were achieved with *p*-type conductivities as high as $\sim 5\ \Omega^{-1}$ cm^{-1} without the presence of Mg-rich inclusions or inversion domains as viewed by cross-section transmission electron microscopy. Temperature dependent Hall effect measurements indicate that the Mg-related acceptor state in *m*-plane GaN is the same as that exhibited in *c*-plane GaN. Free electron concentrations as high as $\sim 4\times 10^{18}$ cm^{-3} were measured in the Si-doped *m*-plane GaN with corresponding mobilities of ~ 500 cm^2/V s measured parallel to the $[11\bar{2}0]$ direction. © *2006 American Institute of Physics*. [DOI: 10.1063/1.2338602]

I. INTRODUCTION

One of the more interesting properties of the wurtzite group-III nitrides is the presence of internal electric fields produced by discontinuities in the spontaneous and piezoelectric polarization along the [0001] axis. While the beneficial and deleterious aspects of the presence of these polarization discontinuities have been, until recently, understood within the context of (0001) oriented films,[1,2] which have historically dominated the literature and commercial applications of the wurtzite group-III nitrides, there has been a large body of recent work on removing and perhaps engineering polarization discontinuities via the growth of nonpolar and semipolar orientations of GaN.[3–5] Growth on inclined facets tilts the polarization toward the plane of the growth surface, thereby reducing the magnitude of the component of the polarization parallel to the growth direction. In the limiting case of *a*-plane $(11\bar{2}0)$ and *m*-plane $(10\bar{1}0)$ orientations, the polarization axis is placed entirely in the plane of the growth surface, and polarization discontinuities at heterointerfaces are not possible.

Though metal organic chemical vapor deposition (MOCVD) has been used to produce the majority of nonpolar and semipolar devices to date, plasma-assisted molecular beam epitaxy (PAMBE) offers a number of advantages over MOCVD when growing a *p*-type material. Typically, Mg is used as a *p*-type dopant in MOCVD. The presence of relatively high concentrations of hydrogen in MOCVD reactors leads to the formation of Mg–H complexes that must be removed by some postgrowth activation method (typically annealing via either direct heating or laser irradiation). PAMBE growth is relatively hydrogen free and the GaN requires no postgrowth activation for Mg-doped samples to exhibit *p*-type conductivity. PAMBE growth of *c*-plane oriented Mg-doped GaN films has also been shown to produce very sharp Mg doping profiles and suffers from no Mg doping memory effect as is commonly observed in MOCVD reactors.[6] Finally, hole concentrations in Mg-doped, MOCVD grown GaN are seen to saturate at high Mg concentrations, perhaps due to the formation of Mg-rich inclusions and compensating point defects. PAMBE grown GaN has not exhibited the formation of inclusions at high doping levels, and the lower growth temperatures of PAMBE may help to suppress compensating point defect formation.

At high Mg doping concentrations (greater than $\sim 1\times 10^{18}$ cm^{-3}) PAMBE grown *c*-plane GaN is prone to the formation of columnar domains of inverted, N-face [i.e., $(000\bar{1})$ oriented] material that extends vertically through the otherwise Ga-face film.[7] These inversion domains are associated with sharp reduction in film conductivity. We have previously reported on our early measurements of *p*-type doping with Mg in PAMBE grown *m*-plane GaN, which show relatively high conductivity films compared to those realized by PAMBE growth of *c*-plane GaN.[8] In this report, we present an expanded analysis of our *m*-plane oriented GaN:Mg films and compare their electrical properties to equivalently doped, uninverted *c*-plane oriented films that have been grown using a method that suppresses the formation of inversion domains for at least moderate levels of Mg incorporation. Because *n*-type doping and structural quality are also important to the production of electrical devices, we also present results from physical characterization of our *m*-plane GaN templates, which were grown on *m*-plane SiC, as well as electrical measurements of Si-doped films.

II. EXPERIMENTAL DETAILS

Samples were grown in a Varian Gen-II MBE system using standard elemental effusion cells for group III and dopant species and active nitrogen produced with a Veeco Unibulb radio-frequency plasma source. The nitrogen plasma source was operated at 275 W with a nitrogen flow rate of 0.3 SCCM (SCCM denotes cubic centimeter per minute at

[a]Electronic mail: mclaurin@engineering.ucsb.edu

STP). These conditions corresponded to a nitrogen limited growth rate of 225 nm/h. Unless otherwise noted, all temperatures reported were measured using a thermocouple located behind the sample. Sample surface temperatures measured by optical pyrometry were ~145 °C higher than those measured via thermocouple.

Mg- and Si-doped *m*-plane GaN samples were grown on unintentionally doped (UID) *m*-plane GaN templates which were grown on commercially available 6*H m*-plane SiC. The SiC substrates were prepared for growth by cleaning in acetone and isopropanol under ultrasonic agitation, followed by a 3 min etch in buffered hydrofluoric acid. The SiC substrates were then bonded with In to Si backing wafers and heated under vacuum to 400 °C for 1 h. The SiC substrates were further cleaned by repeated exposure under vacuum to Ga flux at substrate temperatures similar to those used during growth. Growth was initiated with an approximately 40 nm AlN nucleation layer grown Al rich at 585 °C. The excess Al was then consumed by exposure to only the nitrogen plasma. A 750 nm thick UID GaN film was then grown with Ga excess on the AlN nucleation layer. The UID *m*-plane GaN templates were then removed from vacuum, etched with HCl to remove In and Ga metal, and cleaved into ~1 cm^2 pieces. The UID *m*-GaN templates were prepared for growth by ultrasonic cleaning in acetone, methanol, and isopropanol for 3 min each, bonding with In to a Si backing wafer, and degassing under vacuum at 400 °C for 1 h. Mg-doped GaN Hall effect samples were initiated with an at least 10 nm thick UID GaN buffer layer followed by 500–1000 nm of GaN:Mg grown Ga rich and capped with a 40 nm p^+ GaN layer grown at 480 °C. Si-doped GaN Hall samples were initiated with a 40 nm UID GaN buffer layer followed by ~500 nm of GaN:Si grown Ga-rich. *c*-plane GaN comparison samples were grown Ga rich on commercially available, semi-insulating, Fe-doped templates using equivalent UID buffers and GaN:Mg/p^+ layer thicknesses. The formation of inversion domains in *c*-plane GaN:Mg was suppressed by initiating the growth of the doped layer with an UID buffer grown sufficiently Ga rich to ensure that there was a complete Ga bilayer upon initiation of Mg doping.[9] (0001) oriented GaN:Mg films were determined *in situ* to be "inversion domain free" if they did not exhibit the characteristic 3×3 or 6×6 reconstructions at low temperature (200–300 °C) when imaged with reflection high energy electron diffraction (RHEED). Examples of 3×3 reconstructions from the inverted material are shown in Fig. 1(a), and are easily distinguishable from typical Ga-face 1×1 and 2×2 reconstructions.[7] It is possible to infer the presence of inversion domains from images of the sample surface taken *ex situ* with an atomic force microscope (AFM), especially if the sample has been exposed to an etchant that selectively etches N-face material. A typical example of this is shown in Fig. 1(b), which shows an AFM image of a nominally (0001) oriented, Mg-doped GaN sample that was grown Ga rich and showed 3×3 RHEED reconstructions at low temperature after the growth was terminated. The sample was etched with concentrated HCl in order to selectively etch the N-face regions. Figure 1(c) shows an AFM image of the most highly doped (0001) oriented Mg-doped comparison sample grown in this study. No N-face associated reconstructions were observed in this sample. Etch pits associated with inversion domains have been numbered, and they correspond to an areal density of 2.25×10^6 cm^{-2}. The difference in inversion

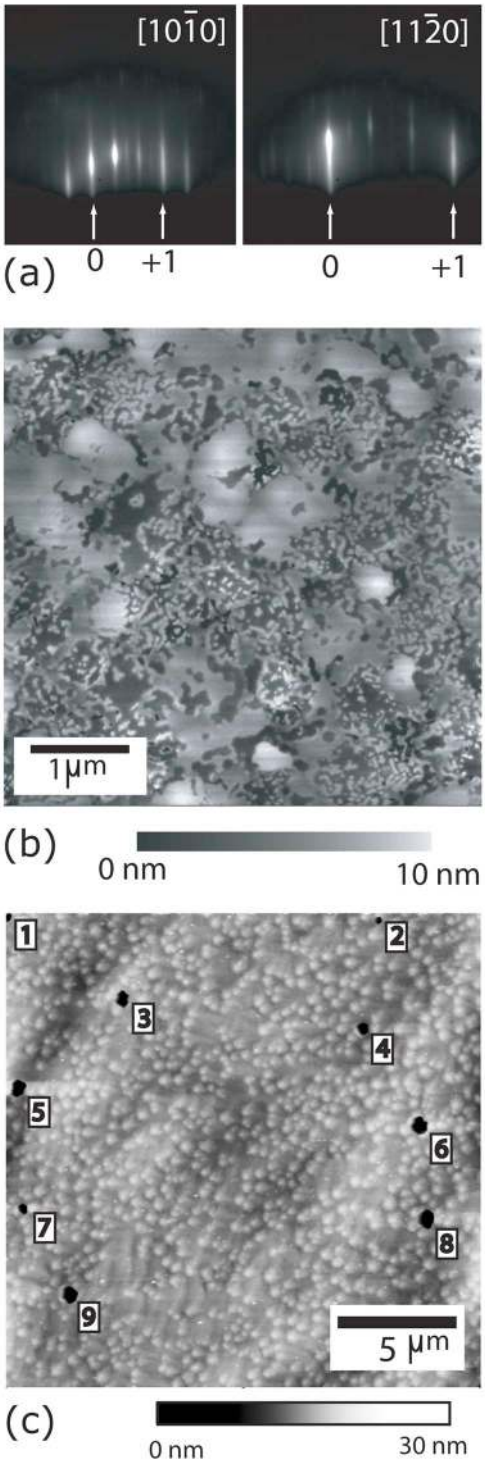

FIG. 1. (a) RHEED images of a nitrogen-face *c*-plane GaN surface showing 3×3 reconstructions characteristic of N-face GaN. Note that the images are taken at azimuthal angles slightly off of the two low-index azimuths to better show the reconstructions. (b) AFM image of a GaN sample grown by PAMBE and intentionally inverted with Mg showing Ga-face material and a high density of inversion domains. (c) AFM image of a Mg-doped (0001) oriented GaN sample grown under inversion suppressing conditions with $[Mg]\sim4.5\times10^{19}$ cm^{-3} and $p\sim1.5\times10^{18}$ cm^{-3}. The sample was etched with concentrated HCl to remove Ga droplets.

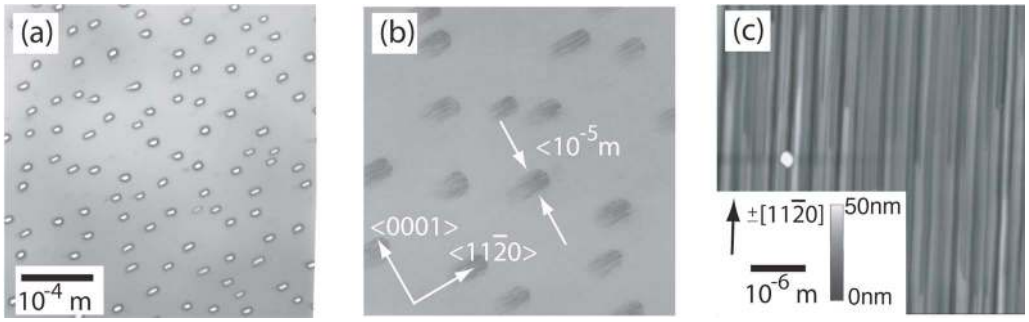

FIG. 2. Micrographs of the *m*-plane GaN template surface: (a) Optical micrograph of post-growth surface showing Ga droplets produced by Ga-rich growth. (b) Optical micrograph of same sample after Ga droplets were removed by etching in HCl. (c) Atomic force micrograph of same sample after HCl etch showing slatelike morphology typical of *m*-plane GaN.

domain size is attributed to the difference in the thicknesses of the layers containing inversion domains (~75 nm versus ~500 nm for the samples in Figs. 1(b) and 1(c), respectively).

Carrier type and concentration were determined from Hall effect measurements. A Hall bar geometry, which is described in Ref. 8, was used with the *m*-plane oriented samples. The sample sheet resistances were derived from linear transfer length method (TLM) measurements (mesa-isolated 100×200 μm^2 contacts with 5–50 μm spacings). Hole mobilities were derived from the measured values of hole concentration and sheet resistance from each film. Both the Hall bars and TLM patterns were oriented parallel to both the [0001] and [11$\bar{2}$0] directions of the *m*-plane surface and were isolated with mesas produced by reactive ion etching. The *c*-plane comparison samples were measured using a mesa-isolated Van der Pauw (VDP) geometry. The Hall and TLM structures were contacted with unannealed 20 nm/200 nm Pd/Au contacts for the Mg-doped samples and 20 nm/200 nm Al/Au contacts for the Si-doped samples. Room temperature Hall effect measurements were made using a Lakeshore Cryotronics 7504 Hall effect system. TLM measurements were made using a Suess MicroTec probe station in conjunction with an HP 4145 semiconductor parameter analyzer. Temperature dependent Hall effect measurements were made using a Quantum Design physical property measurement system. No postgrowth treatment was necessary to electrically activate the Mg. Depth dependent profiles of Mg, Si, C, and O concentrations were measured using secondary-ion-mass spectroscopy (SIMS). SIMS measurements of Mg concentration were calibrated with Mg ion implanted *c*-plane and *m*-plane GaN films. SIMS analysis of Mg-doped samples was performed in both positive and negative ion modes on a Physical Electronics 6650 dynamic SIMS (DSIMS). For negative ion detection, an 8 kV, 300 nA Cs^+ beam was rastered over a 350×450 μm^2 area. For positive ion analysis, a 3 kV O_2^+ beam was rastered over a 300×380 μm^2 area. In both cases, secondary ions were accepted only from the central 15% of the sputtered areas. The system base pressure prior to negative ion analysis was 9×10^{-11} torr. SIMS analysis of Si-doped samples was performed by Charles Evans and Associates using a Cameca SIMS operated with Cs ions at 14.5 keV with negative secondary ion polarity and a conductive gold surface coating. Transmission electron micrographs were taken using a FEI Tecnai G2 Sphera microscope, operated at 200 kV. Atomic force micrographs were obtained using a Digital Instruments Nanoscope IIIA scanning probe microscope operated in tapping mode. X-ray diffraction data were obtained using a Philips X'Pert MRD and Cu $K\alpha_1$ radiation. The x-ray rocking curve scans were measured with an open detector, while all other x-ray data were obtained using a slit aperture.

III. RESULTS AND DISCUSSION

A. *m*-GaN growth on 6*H* *m*-SiC

While growth on lithium aluminate (LAO) has been successful in producing *m*-plane films, LAO is difficult to work with because it can be attacked by water and a number of acids and solvents, and it is less thermally stable than other more conventional substrates for GaN growth. As an alternative to LAO, *m*-plane orient SiC offers a chemically and thermally robust substrate for growth of *m*-plane GaN. SiC, however, is significantly less lattice matched to GaN than LAO, e.g., $[0001]_{GaN}\|[010]_{LAO}$ ~0.3% and $[11\bar{2}0]_{GaN}\|[001]_{LAO}$ ~1.7% (Ref. 10) versus $[0001]_{GaN}\|[0001]_{SiC}$ ~2.9% and $[11\bar{2}0]_{GaN}\|[11\bar{2}0]_{SiC}$ ~3.5%.

Figure 2 shows the surface of an, *m*-plane GaN on SiC film. Figure 2(a) is an optical micrograph showing droplets of Ga formed by the presence of excess Ga during growth. Growth under excess Ga conditions has been shown to be optimal for PAMBE growth of both *m*-plane GaN on LAO (Ref. 10) and *c*-plane oriented films.[11] Figure 2(b) shows the same sample after the excess Ga was removed by etching in HCl. Regions of slatelike morphology can be seen which correspond to the area under droplets. Both Ga droplet formation and roughening of the surface under droplets are typical of PAMBE growth of *c*-plane oriented films. Figure 2(c) is an AFM image of the area located between Ga droplets, and shows a slatelike morphology similar to that seen in growth of *m*-plane GaN on LAO. The RMS roughness for a 25 μm^2 region was ~5.4 nm.

The *m*-plane GaN films were found to be free of (0001) oriented domains. Figure 3(a) shows the x-ray diffraction (XRD) ω-2θ scan of the film shown in Fig. 2. Well-defined peaks corresponding to both the GaN (10$\bar{1}$0) and AlN (10$\bar{1}$0) nucleation layers, can be seen, with no (0001) GaN peak

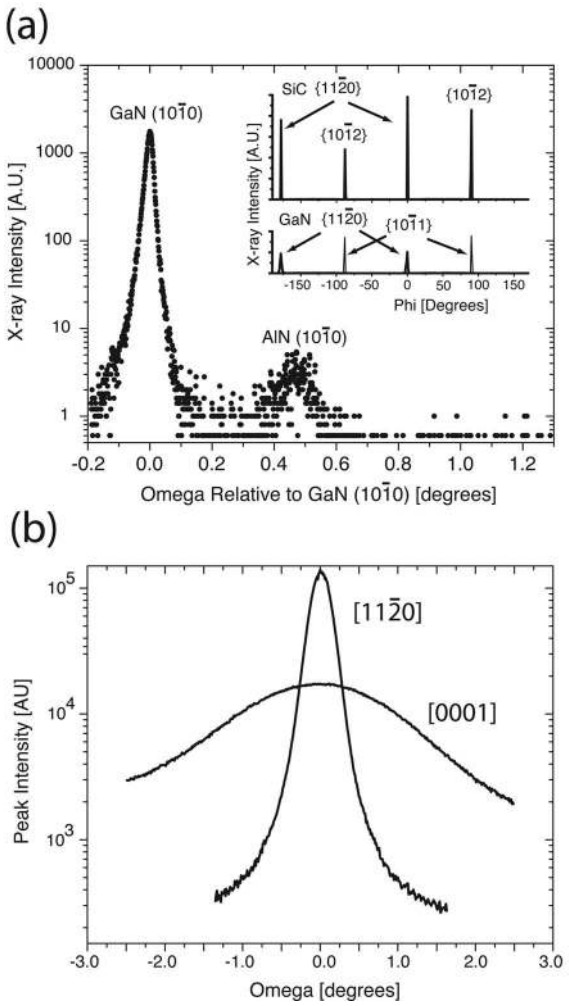

FIG. 3. (a) ω-2θ XRD scan of UID *m*-plane GaN template grown on 6*H* *m*-plane SiC. The inset shows relative peak positions of inclined planes in superimposed XRD φ-scans where the sample has been inclined out of the plane of diffraction by an angle χ (i.e., χ for the GaN $\{11\bar{2}0\}$ and $\{10\bar{1}1\}$ and SiC $\{11\bar{2}0\}$ and $\{10\bar{1}2\}$ are 30°, 28.03°, 30°, and 19.44°, respectively. (b) XRD ω-scan of the *m*-plane GaN (10$\bar{1}$0) peak taken with an open detector parallel to the in-plane [0001] and [11$\bar{2}$0] directions.

present. The *m*-plane GaN films also show the expected orientational relationship with the *m*-plane SiC substrates, e.g., $[0001]_{GaN}\|[0001]_{SiC}$ and $[11\bar{2}0]_{GaN}\|[11\bar{2}0]_{SiC}$, as can be seen by the inset of an XRD phi scan. Figure 3(b) shows XRD rocking curves for the film taken parallel to both the[0001] and [10$\bar{1}$2] directions, which lie in the plane of the sample surface. There is a large anisotropy in the mosaic of the crystal. The full width at half maximum (FWHM) of the rocking curve was ~0.2° parallel to [11$\bar{2}$0] and ~2° parallel to [0001].

Threading dislocations with Burger vectors with nonzero [0001] components were observed in the films by transmission electron microscopy (TEM) at a density of $\sim 2 \times 10^{10}$ cm^{-3}. Basal plane stacking faults were also observed by TEM at a linear density of $\sim 1 \times 10^5$ cm^{-1}. These defect densities are comparable to those found in nonpolar and semipolar films grown by metal organic vapor phase epitaxy[12,13] and hydride vapor phase epitaxy.[14,15]

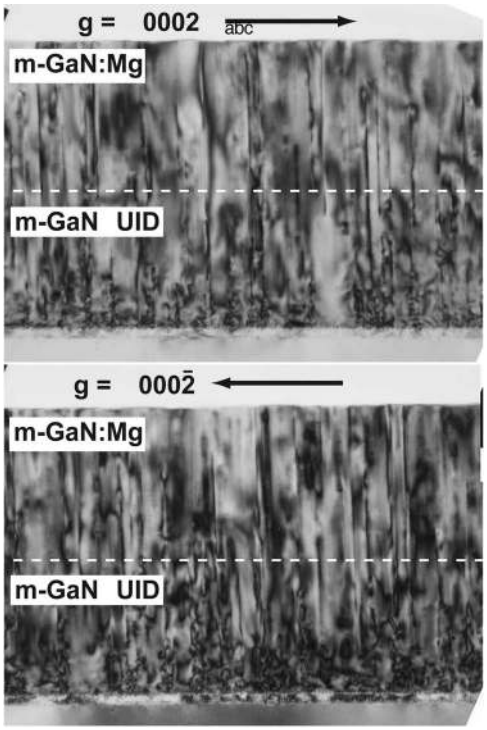

FIG. 4. Bright field transmission electron micrographs of a Mg-doped *m*-plane GaN sample doped with a [Mg]~1.6×10^{20} cm^{-3} and exhibiting a hole concentration of ~710^{18} cm^{-3}. Images for the [11$\bar{2}$0] zone axis under both the $g=0002$ and $g=000\bar{2}$ diffraction conditions are shown. The white dashed line indicates the position of the film where Mg doping was initiated. Beneath the UID GaN layer one can see the AlN nucleation layer and the SiC substrate.

B. Mg-doped *m*-GaN

We previously reported on realizing hole concentrations as high as $\sim 7 \times 10^{18}$ cm^{-3} for *m*-plane Mg-doped GaN films grown on *m*-plane SiC. Typically *c*-plane oriented films with hole concentrations above $\sim 1 \times 10^{18}$ cm^{-3} show saturation or reduction in *p*-type conductivity with increasing Mg concentration. In MOCVD material, saturation in conductivity at high Mg concentrations is related to the presence of either Mg-rich precipitates, inversion domains, or charged, compensating point defects. In MBE grown films the reduction in conductivity is associated primarily with increased scattering due to the formation of inversion domains. Figure 4 shows a transmission electron micrograph of an *m*-plane sample doped with $\sim 1.6 \times 10^{19}$ cm^{-3} Mg, corresponding to a Hall effect derived hole concentration of $\sim 7 \times 10^{18}$ cm^{-3}. Neither inversion domains, precipitates, nor changes in microstructure were observed in the Mg-doped layer compared to the UID material. The absence of inversion domains even at high doping concentrations should not be surprising since the proposed mechanisms for Mg-related inversion in *c*-plane films are believed to be related to the formation of various Mg-rich phases on the [0001] surface.

This interpretation of the micrograph in Fig. 4 implies that the enhanced *p*-type conductivity observed in *m*-plane GaN is the result of the lack of inversion domains rather than the incorporation of Mg into some other, perhaps shallower, acceptor state. To confirm this hypothesis uninverted *c*-plane samples were grown for comparison to the *m*-plane films.

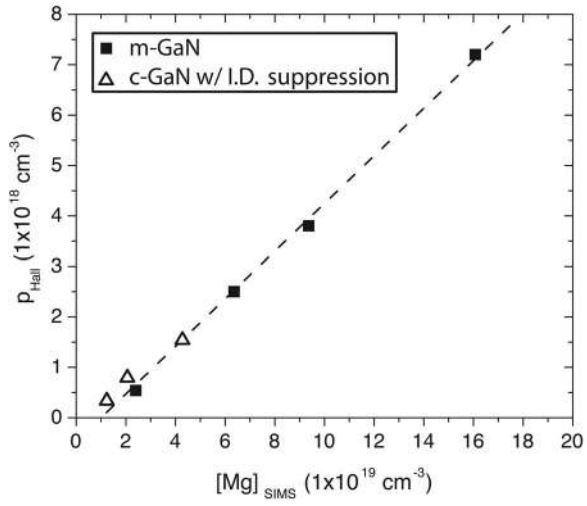

FIG. 5. Dependence of the hole concentration p on the magnesium concentration [Mg] as measured by SIMS for both m-plane samples and c-plane samples grown under inversion domain suppressing conditions. The dashed line is a least-squares fit to the m-plane data.

Figure 5 shows the relationship between hole concentration and SIMS derived Mg concentration in both the m-plane and c-plane films. The agreement between the hole concentration p and the Mg concentration for the two film orientations demonstrates that in both orientations the same fraction of Mg atoms provide holes for conduction and implies that in both orientations the Mg atoms occupy the same acceptor state. Temperature dependent Hall effect measurements were performed on films of both orientations and are presented in Fig. 6. Although the data for the m-plane sample were relatively noisy, it is clear that the activation energy for Mg in m-plane GaN is similar to the 174 meV measured for c-plane GaN. The saturation at low temperature is a characteristic feature of GaN:Mg and is caused by conduction through an,

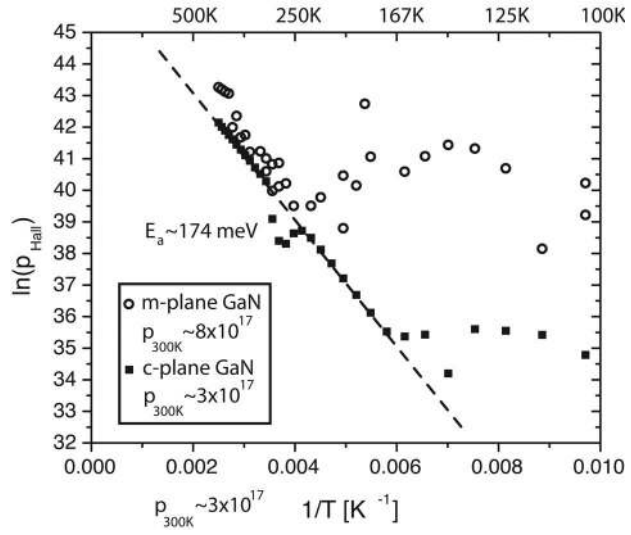

FIG. 6. Temperature dependent Hall measurements for p-type m-plane and c-plane samples exhibiting room temperature hole concentrations of $\sim 8 \times 10^{17}$ and $\sim 3 \times 10^{17}$ cm^{-3}, respectively. The dashed line shows the least squares fit used to extract the c-plane Mg activation energy of $\sim$174 meV. The anomaly located immediately below 300 K is most likely due to changes in the quality of the contacts with temperature.

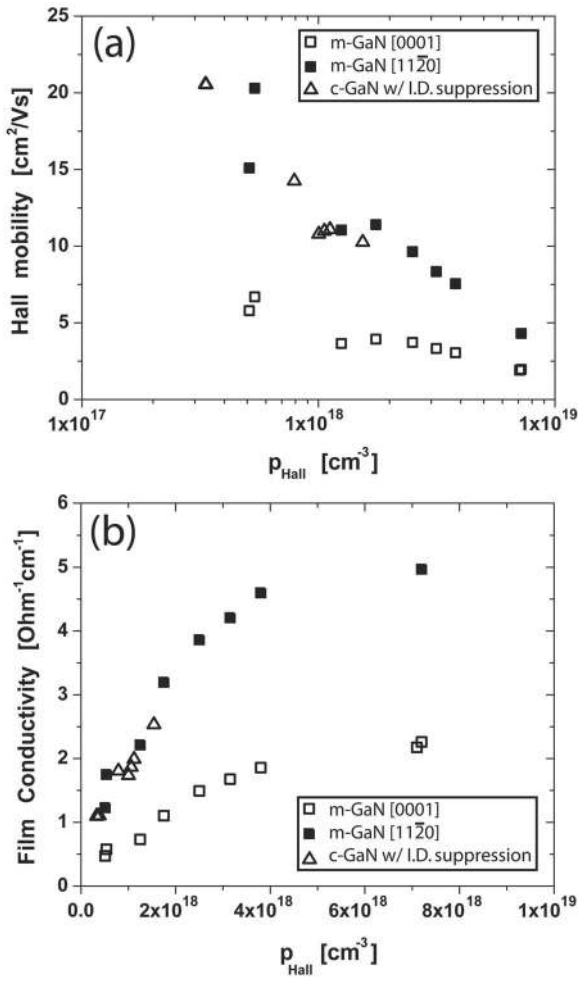

FIG. 7. Electrical measurements of Mg doped m-plane samples and c-plane samples grown using the inversion domain suppression scheme. (a) Hole mobilities for Mg-doped m-plane and c-plane samples measured by a combination of Hall-effect and TLM measurements and Van der Pauw geometry Hall-effect measurements, respectively. In the case of m-plane GaN, hole mobilities parallel to the a and c directions of the surface plane are presented. (b) Dependence of the film conductivity for Mg-doped m-plane and c-plane samples on hole concentration as measured by Hall effect.

impurity band that forms due to the large concentrations of Mg required to achieve appreciable hole concentrations at room temperature.[16]

Figure 7 shows transport properties for a number of Mg-doped m-plane GaN samples. The mobilities measured parallel to both the $[11\bar{2}0]$ and $[0001]$ directions are presented and clearly show anisotropy. Transport properties are also shown for c-plane oriented films grown using the inversion domain suppression method described above. Here we can see that the hole mobility and conductivities in the transverse direction of the c-plane films are in good agreement with those of the a direction in the m-plane films. This should not be surprising, since due to the symmetry of the wurtzite crystal system, all other things being equal, the measurements of electrical properties in the c-plane transverse directions (which include the $[11\bar{2}0]$ and $[10\bar{1}0]$ directions) are isotropic and equivalent to the $[11\bar{2}0]$ direction of m-plane oriented films. The origin of the experimentally observed anisotropy in the in-plane hole mobilities of the m-plane oriented

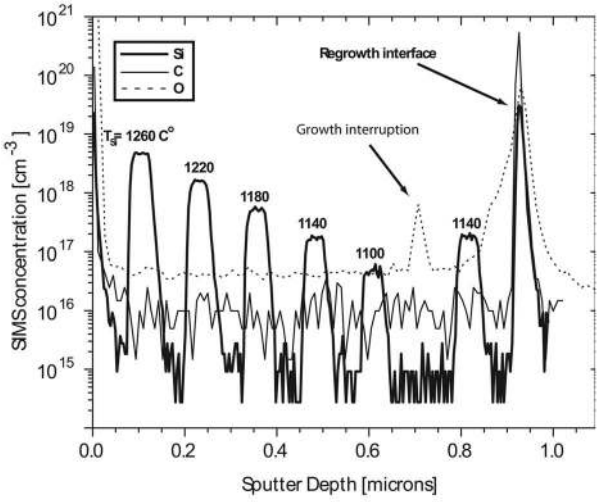

FIG. 8. SIMS depth profiles for a stack of Si-doped layers grown Ga-rich on an *m*-plane GaN template with various silicon cell temperatueres. Unintentional incorporation of O and C is shown to be low and independent of Si-doping concentrations, with the background [O] less than 5×10^{17} cm^{-3} and [C] less than 1×10^{16} cm^{-3}. The positions of the regrowth interface separating the UID GaN template from the intentionally Si-doped GaN as well as a growth interruption where the film was briefly grown N rich are both indicated.

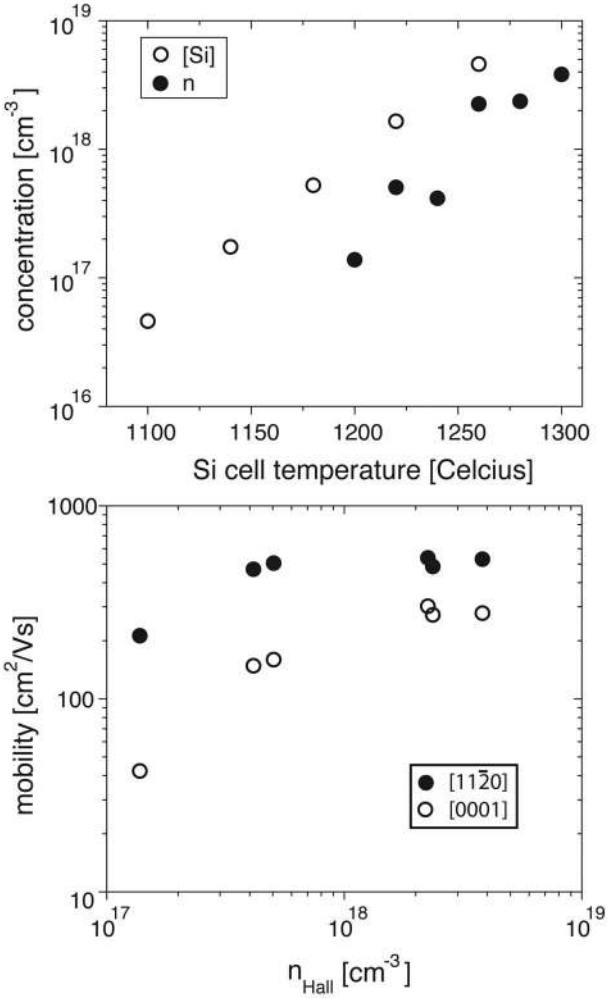

FIG. 9. (a) Dependence of the Si concentration [Si] on the Si cell temperature in *m*-plane GaN. The SIMS data are from the sample shown in Fig. 8. Also shown are Hall effect derived free electron concentrations measured for Si-doped, *m*-plane, *n*-type samples. (b) Dependence of the electron mobility on the free electron concentration for the Hall effect samples shown in part (a).

films is, as yet, undetermined. It is possible, though, to speculate on the origin of the anisotropy. While there is a coincidence of the anisotropies of the film mosaic and hole mobilities, with the *c*-direction having both the lower mobility and larger crystal mosaic, the relative insensitivity of the relatively heavy holes found in GaN to crystal quality makes it doubtful that there is a causal relationship between the two. This is demonstrated best by the good agreement in hole mobility between the *a* direction of the relatively defective *m*-plane films and the transverse direction of the *c*-plane comparison films containing several orders of magnitude lower threading dislocation densities. We speculate the source of the anisotropy to be anisotropy in the effective hole mass.[17,18] Recent calculations show that the ratio of the effective hole masses is highly dependent on the strain state of the film, varying from $m_z/m_x\sim7$ for an unstrained film to $m_z/m_x\sim1.2$ when thermal strain between the GaN film and the SiC substrate is considered.[19]

C. Si-doped *m*-GaN

To study the *n*-type doping of *m*-plane GaN, Si doped samples were grown on MBE grown *m*-GaN templates. Figure 8 shows SIMS depth profiles of Si, O, and C for a sample grown Ga rich at a fixed substrate temperature consisting of alternating layers of UID material and intentionally Si-doped GaN. The results in Fig. 8 demonstrate that sharp Si doping profiles were achieved across a large range of Si concentrations (e.g.,5×10^{16}–5×10^{18} cm^{-3}) with no change in unintentional O and C incorporation ($\sim1\times10^{16}$ and $\sim5\times10^{16}$ cm^{-3}, respectively). Figure 9(a) shows the dependence of the room temperature free electron concentrations and Si concentrations on the silicon effusion cell temperature. The discrepancy between the Si and free electron concentrations is indicative of the presence of a significant concentration of electron traps. Figure 9(b) shows electron mobilities for both the [11$\bar{2}$0] and [0001] directions derived from TLM and Hall effect measurements. The notable features of Fig. 9(b) include the anisotropy in free electron mobility and the decrease in electron mobility with decreasing free electron concentration. The anisotropy in mobility may be explained by noting that the relatively light electrons are especially subject to scattering by crystal defects. In this material, as can be seen by the XRD rocking curves in Fig. 2, there is a large anisotropy in crystal mosaic which may lead to enhanced scattering of electrons propagating along the [0001] direction, and the (0001) plane has a high density of stacking faults. While one might expect a difference in effective mass between the [0001] and [11$\bar{2}$0] because of the reduced symmetry of the wurtzite lattice, it has been established that any anisotropy in electron effective mass is negligible.[20]

A possible explanation for the decrease in electron mobility with decreasing carrier concentration can be found in

Weimann *et al.* where edge type threading dislocations in *c*-plane oriented GaN are considered to be lines of deep-acceptor-like traps which are populated by donated electrons, thus producing charged lines that act as scattering centers.[21,22] Their model, which matches reasonably well with experimental results from *c*-plane oriented samples, results in a large amount of Si concentration dependent compensation which is qualitatively similar to that shown in Fig. 9 and in a decrease in electron mobility with decreasing free electron concentration below $\sim 10^{18}$ cm^{-3} due to reduced screening of line charges.

IV. CONCLUSIONS

m-plane oriented GaN films were grown on 6*H* *m*-plane SiC substrates using PAMBE. Hole concentrations as high as $\sim 7.5 \times 10^{18}$ cm^{-3} corresponding to *p*-type film conductivities as high as 5 Ω^{-1} cm^{-1} were grown. From cross-sectional TEM, temperature dependent Hall measurements and comparisons of the *m*-plane films to Mg-doped *c*-plane samples grown under conditions that suppress inversion domain formation, we conclude that the enhanced *p*-type conductivity in *m*-plane Mg-doped films is due to the absence of inversion domains normally observed in highly Mg-doped *c*-plane films. Si-doped *m*-plane films exhibiting *n*-type conduction were grown and exhibited large densities of electron traps and a dependence of electron mobility on doping density that is qualitatively similar to large ($>10^8$ cm^{-2}) threading dislocation densities of *c*-plane films where the dislocations are decorated with electron traps. Anisotropies in both the hole and electron mobilities were observed. We speculate that the hole mobility anisotropy is due primarily to anisotropy in the hole effective mass, while the electron mobility anisotropy is due primarily to anisotropy in the crystal mosaic and extended defect structure in the *m*-plane GaN films.

ACKNOWLEDGMENTS

The authors thank Michael Grundmann for RHEED images of N-face GaN and Joshua Zide for assistance with temperature dependent Hall effect measurements. The authors also thank the Awschalom group for use of the low-temperature measurement system used to make temperature dependent Hall effect measurements. The Awschalom group is supported by the UCSB CNID/DMEA program. This work was supported by the JST/ERATO program at UCSB. This research made use of MRL facilities supported by the National Science Foundation under Award No. DMR05-20415.

[1] T. Takeuchi, S. Sota, M. Katsuragawa, M. Komori, H. Takeuchi, H. Amano, and I. Akasaki, Jpn. J. Appl. Phys., Part 2 **36**, L382 (1997).
[2] V. Fiorentini, F. Bernardini, F. Della Sala, A. DiCarlo, and P. Lugli, Phys. Rev. B **60**, 8849 (1999).
[3] H. M. Ng, Appl. Phys. Lett. **80**, 4369 (2002).
[4] P. Waltereit, O. Brandt, M. Ramsteiner, R. Uecher, P. Reiche, and K. H. Ploog, J. Cryst. Growth **218**, 143 (2000).
[5] T. J. Baker, B. A. Haskell, F. Wu, P. T. Fini, J. S. Speck, and S. Nakamura, Jpn. J. Appl. Phys., Part 2 **44**, L920 (2005).
[6] I. P. Smorchkova *et al.*, Appl. Phys. Lett. **76**, 718 (2000).
[7] V. Ramachandran, R. M. Feenstra, W. L. Sarney, L. Slamanca-Riba, J. E. Northrup, L. T. Romano, and D. W. Greve, Appl. Phys. Lett. **75**, 808 (1999).
[8] M. Mclaurin, T. E. Mates, and J. S. Speck, Appl. Phys. Lett. **86**, 262104 (2005).
[9] D. S. Green, E. Haus, F. Wu, L. Chen, U. K. Mishra, and J. S. Speck, J. Vac. Sci. Technol. B **21**, 1804 (2003).
[10] Y. J. Sun, O. Brandt, and K. H. Ploog, J. Vac. Sci. Technol. B **21**, 1350 (2003).
[11] B. Heying, I. Smorchkova, C. Poblenz, C. Elsass, P. Fini, S. DenBaars, U. Mishra, and J. S. Speck, Appl. Phys. Lett. **77**, 2885 (2000).
[12] M. D. Craven, F. Wu, A. Chakraborty, B. Imer, U. K. Mishra, S. P. DenBaars, and J. S. Speck, Appl. Phys. Lett. **84**, 1281 (2004).
[13] M. D. Craven, S. H. Lim, F. Wu, J. S. Speck, and S. P. DenBaars, Appl. Phys. Lett. **81**, 469 (2002).
[14] B. A. Haskell, A. Chakraborty, F. Wu, H. Sasano, P. T. Fini, S. P. DenBaars, J. S. Speck, and S. Nakamura, J. Electron. Mater. **34**, 357 (2005).
[15] T. J. Baker, B. A. Haskell, F. Wu, P. T. Fini, J. S. Speck, and S. Nakamura, Jpn. J. Appl. Phys., Part 2 **44**, 1920 (2005).
[16] D. Lancefield and H. Eshghi, J. Phys.: Condens. Matter **13**, 8939 (2001).
[17] Y. C. Yeo, T. C. Chong, and M. F. Liu, J. Appl. Phys. **83**, 1429 (1998).
[18] A. V. Rodina, M. Dietrich, A. Göldner, L. Eckey, A. Hoffmann, Al. L. Efros, M. Rosen, and B. K. Meyer, Phys. Rev. B **64**, 115204 (2001).
[19] H. R. Eisenberg, P. Waltereit, M. McLaurin, H. T. Grahn, S. F. Chichibu, J. S. Speck (unpublished).
[20] I. Vurgaftman and J. R. Meyer, J. Appl. Phys. **94**, 3675 (2003).
[21] N. G. Weimann, L. F. Eastman, D. Doppalapudi, H. M. Ng, and T. D. Moustakas, J. Appl. Phys. **83**, 3656 (1997).
[22] D. C. Look and J. R. Sizelove, Phys. Rev. Lett. **82**, 1237 (1999).